nature chemistry

ARTICLES

PUBLISHED ONLINE: 9 OCTOBER 2011 | DOI: 10.1038/NCHEM.1155

Direct observation of disulfide isomerization in a single protein

Jorge Alegre-Cebollada[1]*, Pallav Kosuri[2], Jaime Andrés Rivas-Pardo[1,3] and Julio M. Fernández[1]*

Photochemical uncaging techniques use light to release active molecules from otherwise inert compounds. Here we expand this class of techniques by demonstrating the mechanical uncaging of a reactive species within a single protein. We proved this novel technique by capturing the regiospecific reaction between a thiol and a vicinal disulfide bond. We designed a protein that includes a caged cysteine and a buried disulfide. The mechanical unfolding of this protein in the presence of an external nucleophile frees the single reactive cysteine residue, which now can cleave the target disulfide via a nucleophilic attack on either one of its two sulfur atoms. This produces two different and competing reaction pathways. We used single-molecule force spectroscopy to monitor the cleavage of the disulfides, which extends the polypeptide by a magnitude unambiguously associated with each reaction pathway. This allowed us to measure, for the first time, the kinetics of disulfide-bond isomerization in a protein.

Disulfides, formed by the oxidation of the sulfhydryl groups of two cysteine residues, are the most widespread cross-links in proteins. In contrast to other covalent bonds, disulfides can be highly dynamic in physiological conditions as a consequence of a set of reactions known as thiol–disulfide exchanges[1]. In these reactions, electrons are reshuffled between a thiolate (R^1–S^-) and a disulfide bond (R^2–S–S–R^3) via an S_N2 mechanism that produces a different disulfide and a new thiolate[2] (Fig. 1a). The relative rate of reactions (1) and (2) in Fig. 1a is referred to as the regiospecificity of the reaction, a concept of the highest importance in thiol–disulfide exchanges in biology. Crucial cellular processes, such as the acquisition of native disulfide bonds of proteins in the endoplasmic reticulum, involve regiospecific thiol–disulfide exchange reactions[3,4].

Although the interaction between redox agents and proteins that contain only one disulfide bond is relatively straightforward, a much more complex scenario is predicted for proteins with multiple disulfides (~19% of proteins). For example, when a disulfide in a protein with more than one disulfide bond is reduced, reactive cysteine residues are generated that can react with the remaining disulfides, which leads to disulfide isomerization. As a result of their general inability to differentiate isomers with the same oxidation state, current bulk techniques have serious limitations in discriminating parallel intramolecular reaction pathways. These bulk approaches usually rely on quenching agents to freeze thiol–disulfide exchange reactions at specific times. Subsequently, the reaction mixtures are analysed by means of techniques such as high-performance liquid chromatography, electrophoresis or NMR spectroscopy[1,4]. Even though smart experimental protocols and careful analysis of the results provide average rates for intramolecular thiol–disulfide exchange, the values obtained span several orders of magnitude[5–7]. In addition, frequently divergent interpretations are given to the experimental results[8,9]. Furthermore, when studying the kinetics of a thiol–disulfide exchange, bulk techniques have to deal with the unavoidable interference from the reverse reaction. Hence, the prevalence of disulfide isomerization reactions in proteins remains to be quantified unambiguously. To this end, it is necessary to obtain unequivocal and regiospecific rates for discrete thiol–disulfide exchange reactions that occur within proteins.

In this work, we report the first direct observation of disulfide isomerization in a protein. We caged a reactive cysteine residue in a protein disulfide and, using single-molecule force-clamp spectroscopy, we freed the reactive cysteine and studied its regiospecific reactivity towards a second disulfide. Different reaction pathways were distinguished by their different associated extensions of the polypeptide chain. Our experimental approach has allowed the first unambiguous description of the kinetics of intramolecular isomerization of disulfides in proteins. Thus, using our new single-molecule methodology, it becomes possible to dissect the increased complexity in thiol–disulfide exchange reactions in polypeptides with more than one disulfide.

Results

Increased complexity in the reduction of a protein with two disulfides. In previous reports, we showed that single-molecule force-clamp spectroscopy by atomic force microscopy (AFM) can monitor the reduction of single disulfides in real time[10,11]. When proteins that contain a disulfide are unfolded under forces of a few hundreds of piconewtons, the unfolding extends up to the disulfide (Fig. 1b). Similar to most other covalent bonds, disulfides cannot be broken by forces below ~1 nN (refs 10,12). Only if a reducing agent is present in solution can the disulfide be cleaved, which is detected as an additional extension of the polypeptide chain. Importantly, the magnitude of this extension is determined solely by the number of amino acids trapped behind the disulfide[13] (Supplementary Information). Furthermore, the reaction is irreversible when studied under force, as both cysteines become separated after the extension of the polypeptide. Thus, the kinetics of the reaction can be monitored with no interference from the reverse reaction. Figure 1c,d shows experimentally obtained reduction events from two polyproteins (that is, single polypeptide chains composed of several modules of the same protein molecule) that consisted of I27 domains with a single disulfide bond, $(I27^{32-75})_8$ (Fig. 1c) and $(I27^{24-55})_8$ (Fig. 1d), in

[1]Department of Biological Sciences, Columbia University, Northwest Corner Building, 550 West 120 Street, New York, New York 10027, USA, [2]Department of Biochemistry and Molecular Biophysics, Columbia University, Northwest Corner Building, 550 West 120 Street, New York, New York 10027, USA, [3]Departamento de Biología, Facultad de Ciencias, Universidad de Chile, Casilla 653, Santiago, Chile. *e-mail: ja2544@columbia.edu; jfernandez@columbia.edu

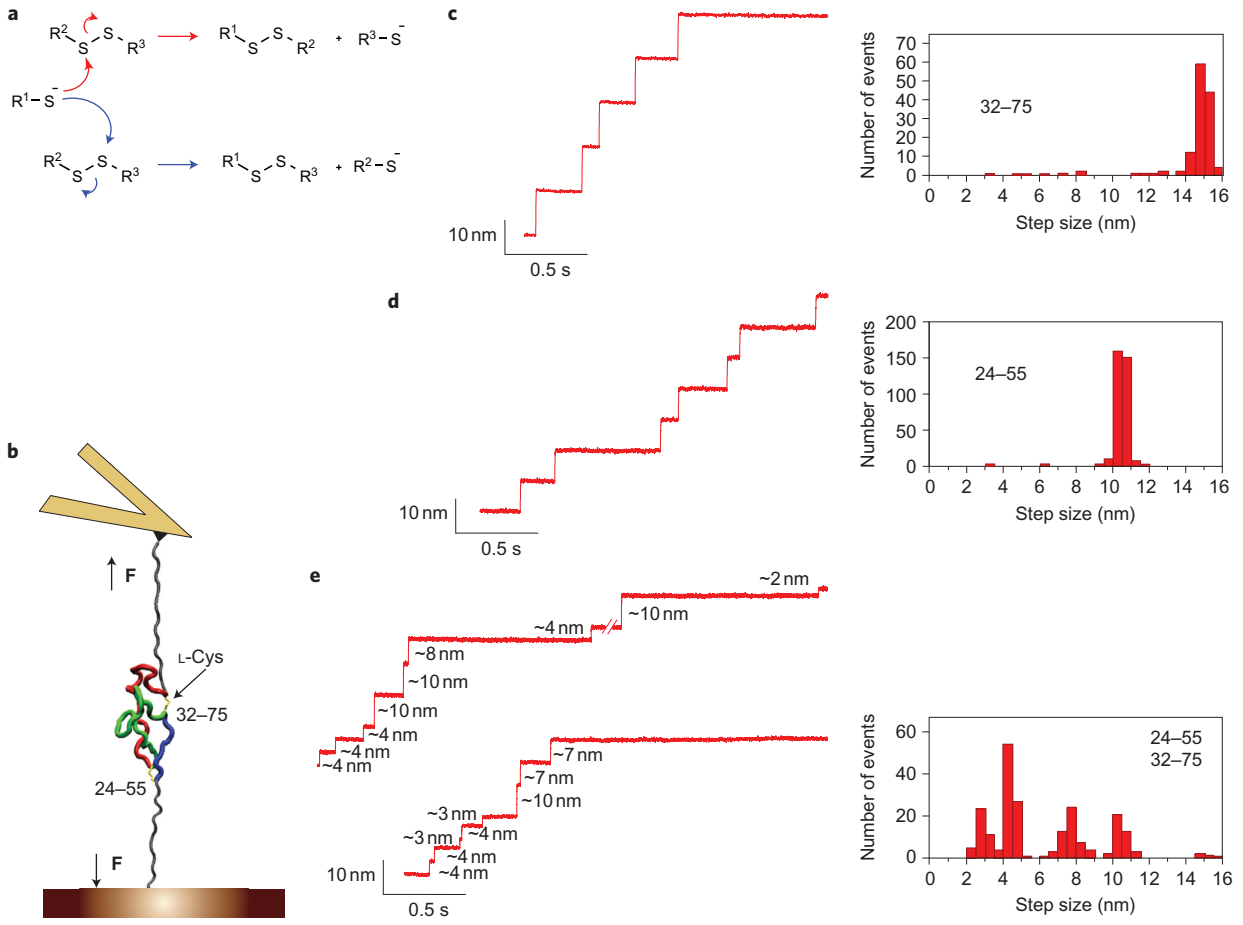

Figure 1 | Increased complexity in the reduction of a protein with two disulfides. a, Generic thiol–disulfide exchange reactions. **b**, Schematic experimental set-up. Polyproteins that contain several I27 modules with one or two disulfide bonds are unfolded by force-clamp AFM. For the sake of simplicity, only a single I27 module is shown. The depicted I27 module ($I27^{2S-S}$) contains two disulfide-linking positions, 24–55 and 32–75. After mechanical unfolding, the disulfides are rendered solvent accessible and can be cleaved by L-Cys. **c**, Experimental trace (left) showing reduction events obtained for $(I27^{32-75})_8$ polyprotein in the presence of L-Cys at 250 pN. The reduction events found for $(I27^{32-75})_8$ are characterized by a single population of 14.5 nm steps (right). **d**, Experimental trace (left) showing reduction events obtained for $(I27^{24-55})_8$ polyprotein in the presence of L-Cys at 250 pN. The step sizes for the reduction events found for $(I27^{24-55})_8$ fall into a single population centred at 10 nm (right). **e**, Two experimental traces (left) showing reduction events obtained for $(I27^{2S-S})_4$ polyprotein in the presence of L-Cys at 250 pN. The distribution of step sizes for the reduction events found for $(I27^{2S-S})_4$ is not a simple combination of the populations found for the proteins with only one disulfide (right).

the presence of L-Cys and at a force of 250 pN. A single population of reduction events was detected at 14.5 nm for $I27^{32-75}$ and 10 nm for $I27^{24-55}$ (Fig. 1c,d). As expected, both experimental values match the predicted ones (Supplementary Information). To study the increase in complexity in the reduction of a protein with multiple disulfides, we performed the same experiment on a polyprotein containing I27 modules with both disulfides 24–55 and 32–75, $(I27^{2S-S})_4$ (Fig. 1b, Supplementary Figs S1 and S2). The results we obtained for $(I27^{2S-S})_4$ (Fig. 1e) cannot be explained by the simple combination of step sizes found for the single-disulfide I27 variants (Fig. 1c,d). On the contrary, the presence of both disulfide bonds in $I27^{2S-S}$ generated a much more complex distribution of step sizes, with at least four different populations centred at 2–3, 4, 7–8 and 10 nm (Fig. 1e).

Force-clamp spectroscopy detects specific disulfide isomerization reactions. We hypothesized that the increase in complexity found in the reduction by L-Cys of $I27^{2S-S}$ could arise from intramolecular thiol–disulfide exchange reactions. To quantify the kinetics of these isomerization reactions, it was first necessary to assign the experimental reduction steps to specific thiol–disulfide exchange reactions. With this aim, we took advantage of the fact that the step sizes of disulfide reduction detected in force-clamp spectroscopy can be predicted from the number of amino acids released after cleavage of the disulfide[13] (Supplementary Information).

The most prevalent step found in the reduction of $I27^{2S-S}$ is characterized by an increase in length of 4 nm. We observed that these steps tended to happen before other events, which suggests that they mark the initial event in the reduction of an $I27^{2S-S}$ domain (Figs 1e and 2). The reduction of disulfide 32–75 in $I27^{2S-S}$ would release 12 amino acids, corresponding to a 4 nm elongation of the polypeptide chain (Supplementary Fig. S3). In contrast, the initial reduction of 24–55 could not produce a 4 nm step (Supplementary Fig. S4). Therefore, we assigned the 4 nm steps to the reduction of disulfide 32–75 in $I27^{2S-S}$.

Immediately after cleavage of disulfide 32–75, Cys75 is pulled away by force and Cys32 remains in the vicinity of disulfide 24–55 (Fig. 2 and Supplementary Fig. S3). Thus, disulfide 24–55 can be cleaved via three different reaction pathways (Fig. 2). As demonstrated above for $I27^{24-55}$, the straightforward reduction of disulfide 24–55 by an external L-Cys molecule extended the protein by 10 nm (Figs 1d and 2a). However, if instead of L-Cys, Cys32 attacks disulfide 24–55 at Cys55, the protein is extended by 3 nm (predicted extension 2.8 nm). This reaction generates a new

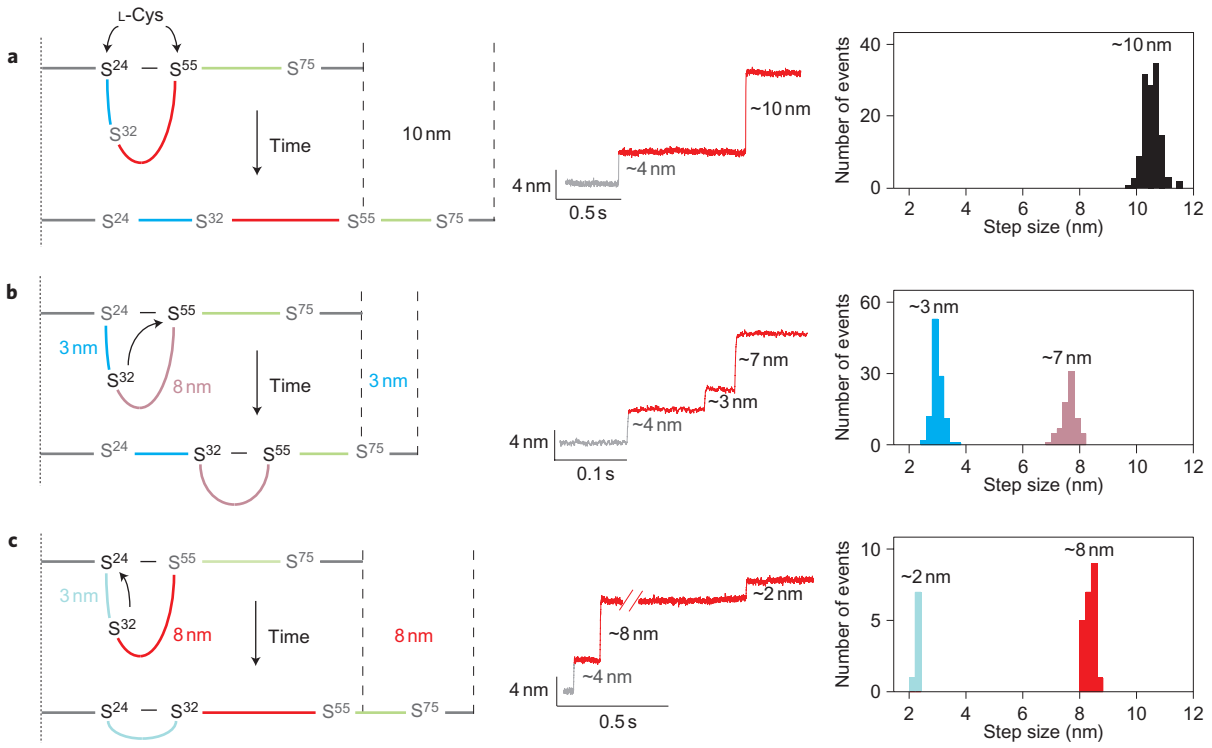

Figure 2 | Fingerprints of the pathways available for the reduction of disulfide 24–55 after the reduction of disulfide 32–75. a–c, In ~95% of the events, disulfide 32–75 in $I27^{2S-S}$ is reduced before disulfide 24–55 to produce a step of 4 nm (Supplementary Fig. S3). After the initial reduction of disulfide 32–75, disulfide 24–55 can be cleaved via three different reaction pathways: cleavage of disulfide 24–55 by L-Cys (**a**), cleavage of disulfide 24–55 by the attack of Cys32 on position 55 (**b**), cleavage of disulfide 24–55 by the attack of Cys32 on position 24 (**c**). The left column illustrates the reaction pathways, the central column shows representative experimental traces and on the right are computed histograms of the step sizes associated with each one of the thiol–disulfide exchanges. The step sizes for different reactions rarely overlap. Hence, the different step sizes together with the order in which the events are detected can be used to assign reaction pathways. In the diagrams on the left, the coloured lines between residues 24 and 32 (blue), 32 and 55 (red), and 55 and 75 (green) represent the polypeptide chain that links the various cysteine residues. The remaining polypeptide chain is depicted in grey. The same colour code is used in Figs 1b and 4a.

disulfide bond, 32–55, that is not present in $I27^{2S-S}$ (Fig. 2b). Alternatively, if Cys32 reacts with the sulfur at Cys24, an 8 nm increase in length was observed (predicted extension 8.1 nm). In this case, the reaction renders a disulfide between residues 24 and 32 (Fig. 2c). Whenever the reduction of disulfide 24–55 was mediated by Cys32, a second step that resulted in the 10 nm total extension followed the initial 3 or 8 nm steps, which indicates the cleavage of the newly isomerized disulfide by an external L-Cys molecule (Fig. 2b,c). Thus, the different regiospecific thiol–disulfide exchange reactions described in Fig. 2 explain the different populations of step sizes found in the reduction of $I27^{2S-S}$ (Fig. 1e). The three pathways start with the cleavage of disulfide 32–75 to render a 4 nm step. The events detected afterwards are a signature of the particular reduction pathway. Two of the reactions are intramolecular thiol–disulfide exchanges, which had not been observed directly before. To assign unambiguously the different step sizes to any of the possible reaction pathways, both the size of the steps and the order in which they appear in a trace were employed (Figs 1e and 2).

Kinetic characterization of the intramolecular isomerization of disulfides. To obtain information about the kinetics of the reactions, we developed a model to account for all the possible reaction pathways for the reduction of $I27^{2S-S}$ by L-Cys, including the regiospecificity of two of the reactions (Fig. 3a; a full description is given in the Supplementary Information). Our model predicts that the frequency of appearance of the different steps is governed both by the corresponding rate constants and the concentration of L-Cys. For example, the first-order constants k_1 and k_7 at a given concentration of L-Cys determine the rate of appearance of the 4 nm steps. However, the appearance of the 10, 3 and 8 nm steps is a much more complex scenario. First, they only happen after a 4 nm step, so their frequency depends on the rate of occurrence of the 4 nm steps. In addition, as they are the signature of competing reaction pathways, their frequency not only depends on their characteristic rate constants, but also on the competing constants. Despite this complexity, the model implies a simple expected behaviour: at high concentrations of L-Cys the frequency of the 10 nm steps should increase at the expense of the 3 and 8 nm steps. This is a direct consequence of the competition between inter- and intramolecular thiol–disulfide exchange reactions, with the former being accelerated by increasing concentrations of external L-Cys (Fig. 3a, top). In addition, the relative frequency of the 3 and 8 nm steps should be independent of the concentration of L-Cys, as both pathways are purely intramolecular. Thus, to test the validity of the kinetic model, we monitored the reduction of $I27^{2S-S}$ in the presence of increasing concentrations of L-Cys. We computed the frequency of appearance of the 10, 3 and 8 nm steps. As predicted by our model, at high concentrations of L-Cys the 10 nm steps became more prevalent and the 3 and 8 nm steps appeared less frequently (Fig. 3b,c). At the same time, the relative frequency of the 3 and 8 nm steps was independent of the concentration of L-Cys (Fig. 3d).

To quantify the rate of the reactions, we computed the dwell times associated with every type of event (Supplementary Fig. S2). Time courses of appearance of the different step sizes were generated by plotting the cumulative number of events at each

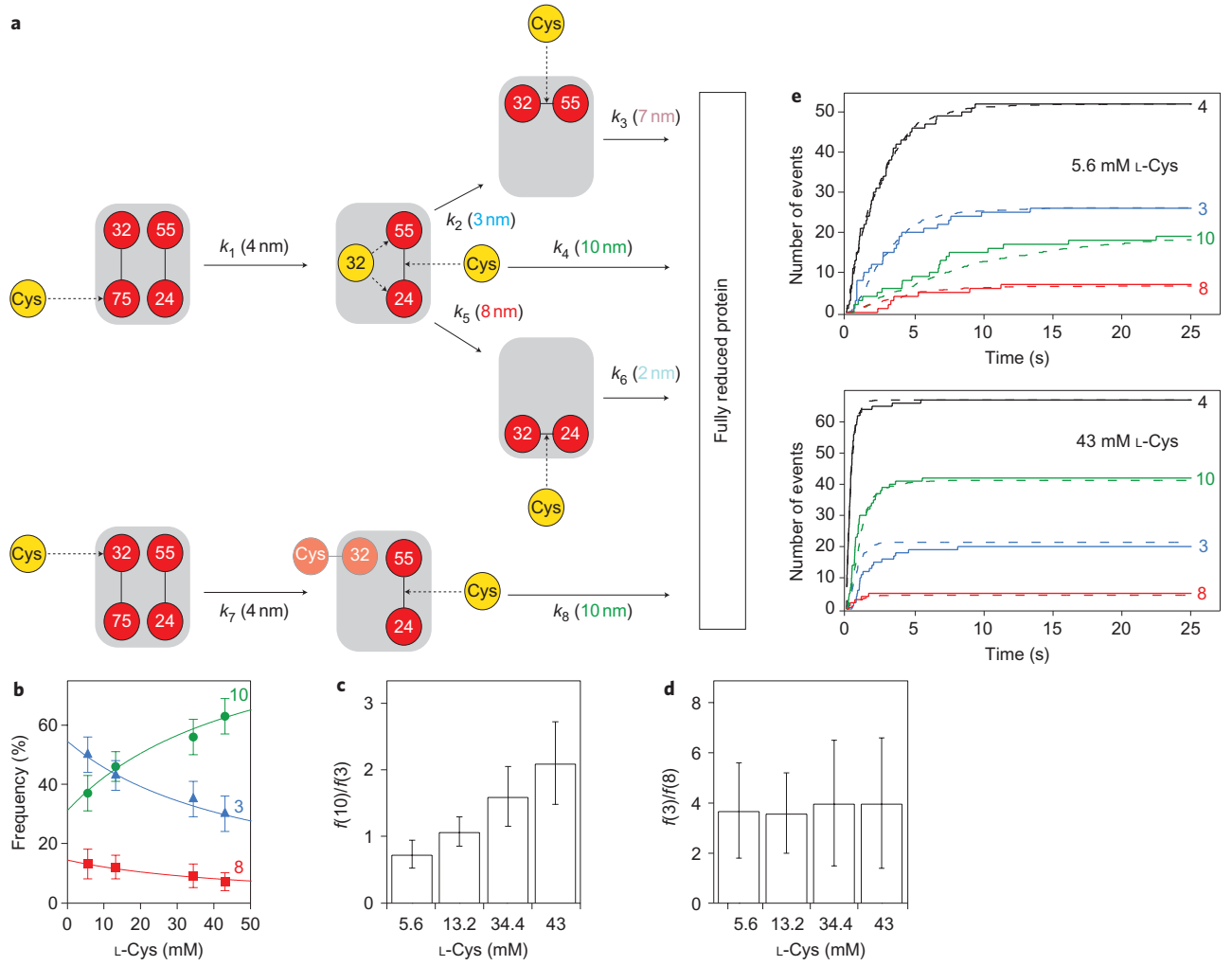

Figure 3 | Kinetic model of complete protein reduction by L-Cys following the initial reduction of disulfide 32–75. a, L-Cys can react with either sulfur in disulfide 32–75. Reaction at position 75 (top) generates a free thiolate at position 32, which can then react intramolecularly with disulfide 24–55. This attack can involve either sulfur atom and competes with the intermolecular reaction with L-Cys. The intramolecular reactions generate new disulfides that can be cleaved only by L-Cys. If the initial reaction happens at position 32 (bottom), the intramolecular reactions are blocked by the formation of a mixed disulfide between L-Cys and Cys32. In this case, a free thiol group is generated at position 75, but it is pulled away by force and cannot participate in intramolecular exchanges with disulfide 24–55. The rate constants that govern the reactions and their characteristic step sizes are indicated. **b**, The frequency of appearance of the step sizes depends on the concentration of L-Cys. The solid lines are the plots of Supplementary equations (S4)–(S6) using rate constants determined employing the downhill simplex method. **c**, With increasing concentrations of L-Cys, the relative frequency of appearance of the 10 and 3 nm steps ($f(10)/f(3)$) increases. **d**, The relative frequency of the 3 and 8 nm steps is independent of L-Cys concentration. The error bars in **b**–**d** were estimated by bootstrapping (see Methods for details). **e**, The solid lines show the time course for the appearance of the different step sizes at two L-Cys concentrations. The dashed lines show the theoretical curves obtained from the rate constants determined using the downhill simplex method. In (**b**) and (**e**), traces are identified by the magnitude of the steps.

particular dwell time (Fig. 3e and Supplementary Fig. S5). As expected from the end-point results discussed above, we found that the kinetics of appearance of the steps is also highly dependent on the concentration of L-Cys (Fig. 3e). To find the rate constants that best fit our experimental data, we solved the coupled differential equations governing the time evolution of our model system (that is, the probability of the system occupying each of the states depicted in Fig. 3a). We then used a downhill simplex method to find the optimal parameters that minimized the discrepancy between the predicted outcome and the experimental data (Supplementary Information). Using this procedure, we determined a set of rate constants that predict kinetic traces highly similar to the experimental results (Fig. 3e and Supplementary Fig. S5). As a further test, we used these rate constants to plot Supplementary Equations (S4)–(S6). We obtained curves that reproduce accurately the frequencies of appearance of the different step sizes (Fig. 3b).

Discussion

In vivo, thiol–disulfide exchange reactions are highly dynamic and regiospecific, and often involve the participation of transient disulfides[14–17]. These properties generate complex behaviours in proteins with multiple disulfide bonds, such as the intramolecular isomerization of disulfides described in this report. However, so far it has been impossible to predict the extent of these ubiquitous isomerization reactions because no accurate estimates existed for the rate of intramolecular thiol–disulfide exchange that occurs in proteins. This is a consequence of the lack of experimental methods able to dissect parallel reaction pathways and still retain kinetic information[1,4,18].

Our experimental approach bears a resemblance to the photochemical uncaging experiments frequently employed to study biological processes, such as neurotransmitter physiology or Ca^{2+}-mediated cell signalling[19,20]. In our case, we caged Cys32 in the

form of an inert disulfide with Cys75 in $I27^{2S-S}$. After the forced unfolding of $I27^{2S-S}$ in the presence of L-Cys, the reactive Cys32 was uncaged and situated in the vicinity of disulfide 24–55. This allowed us to monitor the three different competing reaction pathways available for cleavage of disulfide 24–55 in a synchronized manner (Fig. 4a). Using an analytical optimization procedure, we obtained the rates for each one of the discrete competing pathways (Fig. 4b). Thus, for the first time, we have measured directly the rate of intramolecular thiol–disulfide exchange reactions in a protein.

Noticeably, our results provide a regiospecific description of two different thiol–disulfide exchange reactions. Regarding the intermolecular cleavage of disulfide 32–75 by L-Cys, we found that Cys75 is attacked 2.2 times more frequently than Cys32 (compare the values of k_1 and k_7 that appear in the Supplementary Text). We also observed that the intramolecular attack of Cys32 on position 55 is 3.8 times more frequent than that on position 24 (Fig. 4b). Thus, both thiol–disulfide exchange reactions showed a considerable regiospecificity, the origin of which is intriguing. Steric effects should not have a strong influence on the reactivity towards an unfolded polypeptide. From a chemical point of view, it has been proposed that the quality of a thiolate as a leaving group is related to its pK_a, with lower pK_a values associated with better leaving groups[2]. The presence of positive residues next to Cys32 and Cys55 suggests that these two cysteines are better leaving groups than their counterparts Cys75 and Cys24 (Supplementary Table S1)[2]. We found that Cys32 is the preferred leaving group when cleaving disulfide 32–75. However, Cys24, and not Cys55, is the most frequent leaving group in the rupture of disulfide 24–55. Therefore, our results demand new theoretical developments that can account for the observed experimental regiospecificities.

The order of magnitude we obtained for the rate of intramolecular thiol–disulfide exchange suggests that the spontaneous intramolecular isomerization of disulfides in proteins can compete effectively with their intermolecular reduction. Indeed, for small reducing agents such as glutathione, the fastest experimental rate constants for protein-disulfide reduction are $\sim 10^2\ M^{-1}\ s^{-1}$ (ref. 21). Given that the concentration of glutathione within cells is 10 mM (ref. 21), a maximum rate of $\sim 1\ s^{-1}$ is predicted for disulfide reduction by glutathione. A similar figure is obtained for the enzyme-catalysed reduction of disulfides[22–24]. Thus, with a rate of $\sim 0.3\ s^{-1}$ (Fig. 4b), the isomerization of disulfides may interfere with physiological redox processes. The existence of this unavoidable competition may help to explain why different mechanisms have evolved to mitigate the harmful effects that arise from undesired intramolecular thiol–disulfide exchange reactions. An interesting example is found in protein disulfide isomerases[25]. The malfunction of any such mechanisms could be responsible for the persistent formation of aberrant disulfides that may trigger unfolding and/or aggregation of proteins. Interestingly, some pathologies, such as familial amyotrophic lateral sclerosis or cataract formation, have been linked to the formation of incorrect disulfides in proteins[26,27].

Our study demonstrates the feasibility of mechanically uncaging reactive thiols that can engage in subsequent thiol–disulfide exchange reactions. We speculate that similar mechanisms may be found as regulatory switches in biological systems because the activity of some proteins is controlled by the oxidation state of specific cysteines[28]. Interestingly, some of these proteins are also subject to mechanical stress that can trigger thiol–disulfide exchanges. For instance, the adhesion activity of the von Willebrand factor is regulated by shear-induced disulfide formation[29].

Specific transfers of electrons between cysteine residues are essential for a myriad of cellular redox systems[14,15,17,30] and their relevance in an increasing number of diseases is starting to be unveiled. Additionally, in the emerging field of nanobioelectronics there is a need to develop nanoscopic biomaterials able to transport electrons in a controlled manner[31–33]. Our results validate a new platform for the study of the complexity of intramolecular thiol–disulfide exchange reactions in proteins with multiple disulfides. The single-molecule approach that we introduce here opens up the possibility to systematic studies on how the environment of cysteine residues in proteins modifies their reactivity[34]. Such information may be useful both to predict the behaviour of cysteines and disulfides in physiological reactions and to engineer proteins with particular electron-reshuffling properties. Our methodology relies on the generation of a reactive thiol group from a buried disulfide. A similar experimental design could potentially be employed to study other chemical reactions that involve thiol groups. The mechanical uncaging of different reactive groups may broaden the applicability of our methodology to other chemical reactions that result in the cleavage of mechanically resistant covalent bonds.

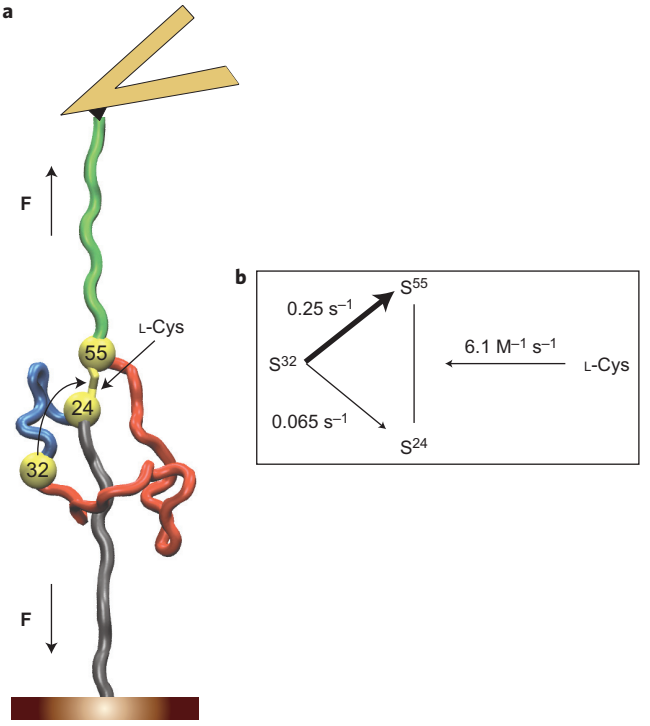

Figure 4 | The uncaging of a single cysteine residue in a protein allows calculation of the rate of spontaneous disulfide isomerization. a, In the presence of external nucleophiles, a single reactive cysteine, Cys32, is uncaged after the mechanical unfolding of $I27^{2S-S}$. Cys32 remains in the vicinity of disulfide 24–55, which can be cleaved by the reaction of any of its sulfur atoms with Cys32 or by the attack of an external L-Cys molecule. **b**, Using our experimental approach, we determined the rates of two intramolecular thiol–disulfide exchange reactions, that is, the attack of Cys32 on Cys24 or Cys55.

Methods

Protein purification. The expression and purification of $(I27^{32-75})_8$ and $(I27^{24-55})_8$ is described elsewhere[13]. To produce the complementary DNA (cDNA) for $I27^{2S-S}$, we applied the QuikChange Multi Site-Directed Mutagenesis kit from Stratagene (La Jolla, California, USA) using the cDNA coding for $I27^{24-55}$ as a template. We constructed polyproteins using an iterative process of digestion and ligation of DNA fragments, as described before[35,36]. BamHI and KpnI sites were used to insert cDNAs into the expression vector pQE80L (Qiagen, Valencia, California, USA)[36]. Protein production in Origami B *Escherichia coli* cells was induced at OD_{600} ~1.0 with 1 mM isopropyl-β-D-thiogalactoside overnight at 23 °C. Soluble proteins were obtained by a combination of sonication and two passes through a French press. Polyproteins were purified from the soluble fraction by affinity chromatography using Talon resin (Mountain View, California, USA), followed by a fast protein liquid chromatography step in a Superdex 200 column (Amersham Biosciences, Pittsburgh, Pennsylvania, USA). The buffer employed was 10 mM HEPES pH 7.2, 1 mM EDTA and 150 mM NaCl. We observed that polyproteins based on I27 modules solely including cysteine residues at positions 24, 32, 55 and

75 were recovered mainly in the insoluble fraction, which precludes purification. However, we found that the amount of soluble proteins could be improved by decreasing the number of repeats in the polyprotein and by mutations that affect the loop between residues 24 and 32. In our experiments, we used a polyprotein with four repetitions of $I27^{2S-S}$, which included the following substitutions at positions 26–30: Ser26-Glu-Pro-Asp-Val30 to Asp26-Asp-Asp-Asp-Lys30. The purification procedure applied to this engineered polyprotein rendered homogeneous soluble fractions of $(I27^{2S-S})_4$, as estimated by sodium dodecyl sulfate polyacrylamide gel electrophoresis (Supplementary Fig. S1).

Single-molecule force-clamp spectroscopy. Aliquots (1–5 μl) of a solution of a $(I27^{2S-S})_4$ (~0.2 mg ml^{-1}) were deposited onto an evaporated gold coverslip. Silicon nitride cantilevers (MLCT, Veeco, Camarillo, CA) were used. They were calibrated using the equipartition theorem[37]. Typical spring constants were in the range 15–25 pN nm^{-1}. To pick up single molecules, the cantilever was pushed against the surface at contact forces of ~2 nN for 1–2 seconds and then retracted. We used a custom-built AFM set-up that allowed a strict control of the force based on an electronic feedback with a ~5 ms response time that controlled the extension of the piezoelectric actuator[38]. Experiments were done at room temperature (22–25 °C) in 10 mM Tris-HCl buffer (pH 7.6). The effective concentration of L-Cys was calculated as described in the Supplementary Information.

Traces with steps that could be assigned to specific thiol–disulfide exchanges were selected. Only traces that showed a pattern of steps compatible with the reaction pathways described in Fig. 2 and Supplementary Fig. S4 (>85% of the selected traces) were included in the analysis. As described elsewhere, the criteria used to select traces in single-molecule force-clamp experiments can affect the calculated rates[39]. For instance, to include traces with short detachment times can bias the results towards faster rates. Consequently, we only considered traces that showed long time intervals between the 4 nm steps and the detachment event (5.6 mM L-Cys, 20 s; 13.2 mM L-Cys, 10 s, 33.4 mM L-Cys, 7.5 s; 43 mM L-Cys, 5 s). These cut-off values were chosen according to slow reaction events observed for each experimental condition.

The error bars in Fig. 3b–d were estimated by bootstrapping[40]. To this end, 10,000 artificial data sets, including the number of observed events for each step size, were generated randomly from the experimental traces at a given L-Cys concentration. Next, the frequency of appearance of each step size was calculated for every simulated data set, which resulted in a distribution of frequencies. The error bars in Fig. 3b are given by the standard deviation of such distributions. The errors in the relative frequencies shown in Fig. 3c,d were calculated from the errors in the corresponding absolute frequencies.

Received 14 April 2011; accepted 23 August 2011; published online 9 October 2011

References

1. Gilbert, H. F. Thiol/disulfide exchange equilibria and disulfide bond stability. *Methods Enzymol.* **251,** 8–28 (1995).
2. Gilbert, H. F. Molecular and cellular aspects of thiol–disulfide exchange. *Adv. Enzymol. Relat. Areas Mol. Biol.* **63,** 69–172 (1990).
3. Mamathambika, B. S. & Bardwell, J. C. Disulfide-linked protein folding pathways. *Annu. Rev. Cell Dev. Biol.* **24,** 211–235 (2008).
4. Wedemeyer, W. J., Welker, E., Narayan, M. & Scheraga, H. A. Disulfide bonds and protein folding. *Biochemistry* **39,** 4207–4216 (2000).
5. Creighton, T. E. & Goldenberg, D. P. Kinetic role of a meta-stable native-like two-disulphide species in the folding transition of bovine pancreatic trypsin inhibitor. *J. Mol. Biol.* **179,** 497–526 (1984).
6. Rothwarf, D. M. & Scheraga, H. A. Regeneration of bovine pancreatic ribonuclease A. 2. Kinetics of regeneration. *Biochemistry* **32,** 2680–2689 (1993).
7. Weissman, J. S. & Kim, P. S. Reexamination of the folding of BPTI: predominance of native intermediates. *Science* **253,** 1386–1393 (1991).
8. Creighton, T. E. The disulfide folding pathway of BPTI. *Science* **256,** 111–114 (1992).
9. Weissman, J. S. & Kim, P. S. Response. *Science* **256,** 112–114 (1992).
10. Wiita, A. P., Ainavarapu, S. R., Huang, H. H. & Fernandez, J. M. Force-dependent chemical kinetics of disulfide bond reduction observed with single-molecule techniques. *Proc. Natl Acad. Sci. USA* **103,** 7222–7227 (2006).
11. Wiita, A. P. *et al.* Probing the chemistry of thioredoxin catalysis with force. *Nature* **450,** 124–127 (2007).
12. Grandbois, M. *et al.* How strong is a covalent bond? *Science* **283,** 1727–1730 (1999).
13. Ainavarapu, S. R. *et al.* Contour length and refolding rate of a small protein controlled by engineered disulfide bonds. *Biophys. J.* **92,** 225–233 (2007).
14. Rozhkova, A. *et al.* Structural basis and kinetics of inter- and intramolecular disulfide exchange in the redox catalyst DsbD. *EMBO J.* **23,** 1709–1719 (2004).
15. van der Neut Kolfschoten, M. *et al.* Anti-inflammatory activity of human IgG4 antibodies by dynamic Fab arm exchange. *Science* **317,** 1554–1557 (2007).
16. Wypych, J. *et al.* Human IgG2 antibodies display disulfide-mediated structural isoforms. *J. Biol. Chem.* **283,** 16194–16205 (2008).
17. Kadokura, H. & Beckwith, J. Four cysteines of the membrane protein DsbB act in concert to oxidize its substrate DsbA. *EMBO J.* **21,** 2354–2363 (2002).
18. Messens, J. *et al.* How thioredoxin can reduce a buried disulphide bond. *J. Mol. Biol.* **339,** 527–537 (2004).
19. Mayer, G. & Heckel, A. Biologically active molecules with a 'light switch'. *Angew. Chem. Int. Ed.* **45,** 4900–4921 (2006).
20. Gorostiza, P. & Isacoff, E. Y. Optical switches for remote and noninvasive control of cell signaling. *Science* **322,** 395–399 (2008).
21. Shaked, Z., Szajewski, R. P. & Whitesides, G. M. Rates of thiol–disulfide interchange reactions involving proteins and kinetic measurements of thiol pK_a values. *Biochemistry* **19,** 4156–4166 (1980).
22. Schafer, F. Q. & Buettner, G. R. Redox environment of the cell as viewed through the redox state of the glutathione disulfide/glutathione couple. *Free Radic. Biol. Med.* **30,** 1191–1212 (2001).
23. Holmgren, A. Reduction of disulfides by thioredoxin. Exceptional reactivity of insulin and suggested functions of thioredoxin in mechanism of hormone action. *J. Biol. Chem.* **254,** 9113–9119 (1979).
24. Dyson, H. J. *et al.* Effects of buried charged groups on cysteine thiol ionization and reactivity in *Escherichia coli* thioredoxin: structural and functional characterization of mutants of Asp 26 and Lys 57. *Biochemistry* **36,** 2622–2636 (1997).
25. Hatahet, F. *et al.* Protein disulfide isomerase: a critical evaluation of its function in disulfide bond formation. *Antioxid. Redox Signal* **11,** 2807–2850 (2009).
26. Wang, J., Xu, G. & Borchelt, D. R. Mapping superoxide dismutase 1 domains of non-native interaction: roles of intra- and intermolecular disulfide bonding in aggregation. *J. Neurochem.* **96,** 1277–1288 (2006).
27. Pande, A., Gillot, D. & Pande, J. The cataract-associated R14C mutant of human gamma D-crystallin shows a variety of intermolecular disulfide cross-links: a Raman spectroscopic study. *Biochemistry* **48,** 4937–4945 (2009).
28. Hogg, P. J. Disulfide bonds as switches for protein function. *Trends Biochem. Sci.* **28,** 210–214 (2003).
29. Choi, H. *et al.* Shear-induced disulfide bond formation regulates adhesion activity of von Willebrand factor. *J. Biol. Chem.* **282,** 35604–35611 (2007).
30. Frand, A. R. & Kaiser, C. A. Two pairs of conserved cysteines are required for the oxidative activity of Ero1p in protein disulfide bond formation in the endoplasmic reticulum. *Mol. Biol. Cell* **11,** 2833–2843 (2000).
31. Davis, J. J. *et al.* Molecular bioelectronics. *J. Mater. Chem.* **15,** 2160–2174 (2005).
32. Willner, I. Tech.Sight. Bioelectronics. Biomaterials for sensors, fuel cells, and circuitry. *Science* **298,** 2407–2408 (2002).
33. Birge, R. R. *et al.* Biomolecular electronics: protein-based associative processors and volumetric memories. *J. Phys. Chem. B* **103,** 10746–10766 (1999).
34. Weerapana, E. *et al.* Quantitative reactivity profiling predicts functional cysteines in proteomes. *Nature* **468,** 790–795 (2010).
35. Carrion-Vazquez, M., Marszalek, P. E., Oberhauser, A. F. & Fernandez, J. M. Atomic force microscopy captures length phenotypes in single proteins. *Proc. Natl Acad. Sci. USA* **96,** 11288–11292 (1999).
36. Alegre-Cebollada, J., Badilla, C. L. & Fernandez, J. M. Isopeptide bonds block the mechanical extension of pili in pathogenic *Streptococcus pyogenes*. *J. Biol. Chem.* **285,** 11235–11242 (2010).
37. Florin, E. L. *et al.* Sensing specific molecular-interactions with the atomic-force microscope. *Biosens. Bioelectron.* **10,** 895–901 (1995).
38. Schlierf, M., Li, H. & Fernandez, J. M. The unfolding kinetics of ubiquitin captured with single-molecule force-clamp techniques. *Proc. Natl Acad. Sci. USA* **101,** 7299–7304 (2004).
39. Garcia-Manyes, S., Brujic, J., Badilla, C. L. & Fernandez, J. M. Force-clamp spectroscopy of single-protein monomers reveals the individual unfolding and folding pathways of I27 and ubiquitin. *Biophys. J.* **93,** 2436–2446 (2007).
40. Efron, B. *The Jackknife, the Bootstrap, and Other Resampling Plans* (SIAM, 1982).

Acknowledgements

This work was supported by National Institutes of Health grants HL66030 and HL61228 to J.M.F. J.A-C. thanks Fundación Caja Madrid, Fundación Alfonso Martín Escudero (Madrid, Spain) and Fundación Ibercaja (Zaragoza, Spain) for their financial support. J.A.R-P. is the recipient of a fellowship from la Comisión Nacional de Investigación Científica y Tecnológica and a Programa de Mejoramiento de la Calidad y la Equidad de la Educación Superior visiting scholar fellowship UCH7013 (Chile). We thank J. Li and B.J. Berne for their help with the steered molecular dynamics simulations. We also thank S.G-M. for reading the manuscript.

Author contributions

J.A-C. and J.M.F. designed the research project, J.A-C. and J.A.R-P. performed the experiments, J.A-C., P.K., J.A.R-P. and J.M.F. analysed the data. J.A-C., P.K. and J.M.F. co-wrote the paper.

Additional information

The authors declare no competing financial interests. Supplementary information accompanies this paper at www.nature.com/naturechemistry. Reprints and permission information is available online at http://www.nature.com/reprints. Correspondence and requests for materials should be addressed to J.A-C. and J.M.F.